**Proceedings of the ASME 2012 International Mechanical Engineering Congress & Exposition**
**IMECE2012**
**November 9-15, 2012, Houston, Texas, USA**

# IMECE2012-87675

# CONTINUUM MANIPULATOR STATICS BASED ON THE PRINCIPLE OF VIRTUAL WORK

**William S. Rone**
Robotics and Mechatronics Laboratory
The George Washington University
Washington, DC, USA

**Pinhas Ben-Tzvi**
Robotics and Mechatronics Laboratory
The George Washington University
Washington, DC, USA

## ABSTRACT

This paper presents a generalized method of determining the static shape conformation of a continuum robot based on the principle of virtual work. A lumped parameter model is utilized to model a prototypical single-segment manipulator. Elastic effects, gravitational forces and actuation loading are modeled as generalized forces and moments acting along the manipulators at discrete masses. A brief derivation of the governing static equations based on the principle of virtual work is presented, and then applied to the problem of continuum manipulator statics. The numerical method was successfully implemented numerically, capable of determining a system's static equilibrium given a prescribed actuation.

## KEYWORDS

Continuum robotics, principle of virtual work, statics

## NOMENCLATURE

| | |
|---|---|
| $\boldsymbol{F}$ | Applied force (N) |
| $\boldsymbol{F}_g$ | Gravitational force (N) |
| $\boldsymbol{F}_{ax}$ | Axial force (N) |
| $\boldsymbol{F}_{act}$ | Actuation force (N) |
| $L$ | Segment length (m) |
| $L_0$ | Undeformed segment length (m) |
| $\boldsymbol{M}$ | Applied moment (N-m) |
| $\boldsymbol{M}_b$ | Bending moment (N-m) |
| $\boldsymbol{M}_{act}$ | Actuation moment (N-m) |
| $\boldsymbol{P}$ | Generalized force (N or N-m) |
| $\boldsymbol{T}$ | Local-to-global coordinate transformation (unitless) |
| $W$ | Virtual work (N-m) |
| $g$ | Gravitational acceleration, (m/s$^2$) |
| $k$ | Segment curvature (1/m) |
| $n$ | Number of disks (unitless) |
| $\boldsymbol{p}$ | Disk position and orientation (m and rad) |
| $\boldsymbol{p}_{lcl}$ | Local segment position and orientation (m and rad) |
| $\boldsymbol{p}_0$ | Initial disk position and orientation (m and rad) |
| $\boldsymbol{q}$ | Generalized coordinates (m or rad ) |
| $\boldsymbol{q}_0$ | Undeformed configuration (m or rad) |
| $\boldsymbol{q}^*$ | Single-segment generalized coordinate (m or rad) |
| $\boldsymbol{r}$ | Generalized displacements (m or rad) |
| $\boldsymbol{r}_h$ | Cable routing hole position (m) |
| $x, y$ | Linear displacement coordinates (m) |
| $\boldsymbol{\delta}$ | Linear displacement vector (m) |
| $\boldsymbol{\theta}$ | Angular displacement vector (rad) |
| $\theta$ | In-plane angular rotation (rad) |
| $\tau$ | Prescribed cable tension |

## I. INTRODUCTION

Continuum manipulation is an emerging field within robotics promising to address many shortcomings of conventional rigid-link manipulators. Benefits of continuum manipulation include their inherent compliance when handling delicate objects or interacting with people, the ease of whole-arm manipulation using the entire length of the robotic arm to wrap around the payload, and the greater flexibility of the overall manipulator shape when navigating unstructured environments. However, compared to rigid-link robotics, the analytical work in the scientific literature on modeling of continuum manipulator shape is lacking.

Previous work in modeling the time-invariant shape conformation of continuum manipulators has focused on kinematic and static models. Kinematic models ignore the force-based effects present in the system and formulate relationships based on geometric quantities. In the case of a cable-driven manipulator, given a set of cable displacements, the resulting shape of the manipulator is found simply due to geometric constraint. Webster and Jones [1] provide an exhaustive review of constant-curvature based methods of modeling continuum manipulators, where actuated segments are assumed to exhibit a single constant curvature along its length. Alternatively, Chirikjian and Burdick [2] have presented a method in which manipulators are actuated to shape-fit prescribed Bessel function curves.

Static models utilize a manipulator's mechanics when determining its shape conformation; in the case of a cable-driven manipulator, the cable tensions are considered as inputs. Relevant effects modeled may include elasticity, gravity, actuation force and gravity. Jones *et al*. [3] utilize Cosserat rod theory to represent the manipulator as a one-dimensional curve in space. Rucker *et al*. [4] minimized an energy function to determine the static equilibrium configuration of a continuum manipulator. Xu and Simaan [5] utilized elliptic integrals to model shape, allowing for an analytical solution to the partial differential equations defining the mechanics.

### Significance

In this paper, a novel method of modeling continuum manipulator statics is derived using the principal of virtual work. The method is applied based on a novel method of representing the system as a serial chain of piecewise constant-curvature continuum segments within a single actuated region. This geometry-based discretization better represents the manipulator structure for numerical calculation than an arbitrary mesh defined for the solution of a continuous formulation of mechanics (such as by ordinary differential equations). This work will enable further work in continuum manipulator statics (incorporating additional non-conservative forces such as friction as additional virtual work terms) and dynamics (using the method of virtual power/Kane's method to model system dynamics). Benefits of this method in relation to current method of modeling include: (1) it is a static method that accounts for mechanical effects, unlike kinematic models; and (2) the model results in a series of coupled nonlinear equations, as opposed to a series of coupled ordinary differential equations to be meshed and solved.

### Outline

Section II provides background on the principle of virtual work and the manipulator structure under consider. Section III describes the virtual-work-based continuum manipulator static analysis. Section IV describes the numerical implementation of the method and presents the results. Section V draws conclusions from these results and describes future work associated with this research.

## II. BACKGROUND

In this section, the fundamentals of the principle of virtual work are presented, along with a description of the continuum manipulation segment under consideration.

### Principle of Virtual Work

The principle of virtual work arises as a fundamental result of variational calculus [6]. For a deformable system in static equilibrium, by comparing the static equilibrium configuration to a reference, undeformed configuration, a metric of virtual work $W$ may be constructed by summing the dot products of each generalized force $\boldsymbol{P}_j$ acting on the system with the associated generalized displacement $\boldsymbol{r}_j$, shown in Eq. 1 (a generalized force may be a force or moment).

$$W = \sum_j \boldsymbol{P}_j \cdot \boldsymbol{r}_j \tag{1}$$

Based on the principle of least action, for a system in static equilibrium, $W$ is a minimum value. As a consequence, the first order variation of the work ($\Delta W$) is zero, as shown in Eq. 2. The system is characterized in its joint space by a set of generalized coordinates $\boldsymbol{q}$. The variation in work must remain identically zero regardless of variation in generalized coordinate; this property enables construction of the constraint equations for static equilibrium.

$$\Delta W = \sum_j \boldsymbol{P}_j \cdot \Delta \boldsymbol{r}_j = 0 \tag{2}$$

The variation in generalized displacement $\Delta \boldsymbol{r}_j$ may be related to the variation in generalized coordinates $\Delta \boldsymbol{q}_i$ by a first-order Jacobian mapping, shown in Eq. 3. Applying this mapping to Eq. 2 results in Eq. 4, in which the variation in virtual work is constructed as a weighted sum of the variations in generalized coordinates.

$$\Delta \boldsymbol{r}_j = \frac{\partial \boldsymbol{r}_j}{\partial q_1}\Delta q_1 + \cdots + \frac{\partial \boldsymbol{r}_j}{\partial q_n}\Delta q_n = \sum_i \frac{\partial \boldsymbol{r}_j}{\partial q_i}\Delta q_i \tag{3}$$

$$\Delta W = \left[\sum_j \boldsymbol{P}_j \cdot \frac{\partial \boldsymbol{r}_j}{\partial q_1}\right]\Delta q_1 + \cdots + \left[\sum_j \boldsymbol{P}_j \cdot \frac{\partial \boldsymbol{r}_j}{\partial q_n}\right]\Delta q_n \tag{4}$$

In order for Eq. 4 to remain equal to zero regardless of the variation in generalized coordinate, the coefficients must equal zero, as shown in Eq. 5. These are the governing equations for the static equilibrium.

$$\sum_j \boldsymbol{P}_j \cdot \frac{\partial \boldsymbol{r}_j}{\partial q_i} = 0 \qquad (5)$$

### Continuum Manipulator Structure

In this paper, the mechanics of a cable-driven manipulator with an elastic core are considered. Figure 1 illustrates the typical structure of such a manipulator, based on an implementation by Rucker and Webster [7]. Rigid disks are mounted along an elastic core, and flexible cables transmit actuation along the length of the manipulator. A frictionless interaction is assumed along the length of the cable, resulting in a constant tension along the length of the cable. This assumption is common in the literature during early-stage investigations into continuum robot mechanics [7] and may be validated by selecting low friction materials for the disk and cable (such as Teflon-filled plastic and Teflon-coated thread).

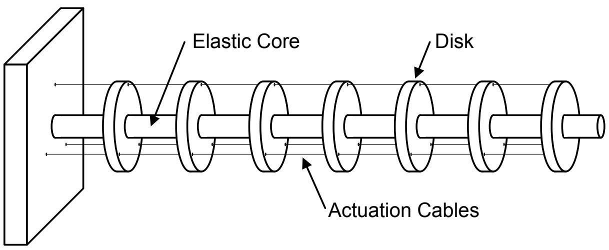


**FIGURE 1. CABLE-DRIVEN MANIPULATOR STRUCTURE**

When calculating the mass of each disk during the analysis, an effective mass accounting for both the disk and the elastic core will be formulated, due to the segment-based discretization of generalized coordinates used to model the system (discussed in Section 3). An alternative cable-driven structure is presented by McMahon et al. [8] with a variable-pressure pneumatic core – with minor adaptations, this analysis is also applicable to that structure.

## III. ANALYTICAL DERIVATION

In this section, the static governing equations for a planar cable-driven continuum manipulator are derived. The system parameterization into a finite set of generalized coordinates is presented, along with kinematic and static analyses.

### System Parameterization

The manipulator is discretized into a series of piecewise arcs of constant curvature. Each segment is parameterized by two generalized coordinates $\boldsymbol{q}^*$: segment curvature $k$ and segment length $L$. The generalized coordinates $\boldsymbol{q}$ of the system may be found by concatenating these segment curvatures together for the $n$ disks of the system (Eq. 6). The initial undeformed configuration of the manipulator is given as $\boldsymbol{q}_0$.

$$\begin{gathered} \boldsymbol{q}^* = \begin{bmatrix} k_i & L_i \end{bmatrix}^T, \\ \boldsymbol{q} = \begin{bmatrix} k_1 & L_1 & \cdots & k_n & L_n \end{bmatrix}^T \\ \boldsymbol{q}_0 = \begin{bmatrix} k_0 & L_0 & \cdots & k_0 & L_0 \end{bmatrix}^T \end{gathered} \qquad (6)$$

The dot product of the generalized forces and partial generalized displacements in Eq. 5 may be represented as the sum of two dot products for each disk $j$: (1) the dot product of the net force acting at each center of mass ($\boldsymbol{F}_j$) with the Jacobian mapping of the corresponding linear displacement at that center of mass ($\partial \boldsymbol{\delta}_j / \partial q_i$), and (2) the dot product of the net moment acting at each center of mass ($\boldsymbol{M}_j$) with the Jacobin mapping of the corresponding angular displacement of that center of mass($\partial \boldsymbol{\theta}_j / \partial q_i$), as shown in Eq. 7.

$$\sum_j \left( \boldsymbol{F}_j \cdot \frac{\partial \boldsymbol{\delta}_j}{\partial q_i} + \boldsymbol{M}_j \cdot \frac{\partial \boldsymbol{\theta}_j}{\partial q_i} \right) = 0 \qquad (7)$$

In this model, the net force at each disk $\boldsymbol{F}_j$ is composed of three terms: the gravitational loading $\boldsymbol{F}_{g,j}$, the axial elastic force $\boldsymbol{F}_{ax,j}$ due to segment compression/extension and the actuation force $\boldsymbol{F}_{act,j}$. The net moment at each disk $\boldsymbol{M}_j$ is composed of the elastic moment $\boldsymbol{M}_{b,j}$ due to segment bending and the actuation moment $\boldsymbol{M}_{act,j}$. Both are shown in Eq. 8.

$$\begin{gathered} \boldsymbol{F} = \boldsymbol{F}_g + \boldsymbol{F}_{ax} + \boldsymbol{F}_{act}, \\ \boldsymbol{M} = \boldsymbol{M}_b + \boldsymbol{M}_{act} \end{gathered} \qquad (8)$$

In order to analyze the actuation force/moment contributions and the displacement/coordinate Jacobian mapping, a kinematic analysis is required to determine the relative positions/orientations between the disks, and the global positions/orientations of the disks.

### System Kinematics

For each disk $i$, three coordinates describe the position/orientation ($\boldsymbol{p}_i$, Eq. 9): two orthogonal linear coordinates $x_i$ and $y_i$, and one angular coordinate $\theta_i$ orthogonal to the plane of linear motion. The initial coordinates of each disk are also shown in Eq. 9: each consists of an x-coordinate based on the disk number $i$, and zero y and z.

$$
\begin{aligned}
\boldsymbol{p}_i &= \begin{bmatrix} \boldsymbol{\delta}_i^T & \boldsymbol{\theta}_i \end{bmatrix}^T = \begin{bmatrix} x_i & y_i & \theta_i \end{bmatrix}^T , \\
\boldsymbol{p}_{0,i} &= \begin{bmatrix} i \cdot L_0 & 0 & 0 \end{bmatrix}^T
\end{aligned} \tag{9}
$$

$\boldsymbol{p}_i$ may be calculated recursively, using the previous segment's position $\boldsymbol{p}_{i-1}$ and the local position $\boldsymbol{p}_{i,lcl}$ due to the segment's bending and extension/compression, as shown in Eq. 10. A coordinate transformation $\boldsymbol{T}_{i-1}$ is utilized to map the local coordinates relative to the disk $i-1$ frame to the global frame. In addition, an expression for the segment $1$ position is required due to the use of backward recursion; because the previous frame for the disk $1$ local coordinates is the global frame, no coordinate transformation is needed.

$$
\begin{aligned}
\boldsymbol{p}_i &= \boldsymbol{p}_{i-1} + \boldsymbol{T}_{i-1}\boldsymbol{p}_{i,lcl} \\
\boldsymbol{p}_1 &= \boldsymbol{p}_{1,lcl}
\end{aligned} \tag{10}
$$

A geometric argument may be used to formulate the coordinates of the segment endpoint based on the segment's generalized coordinates. Figure 2 illustrates a single segment's geometry and demonstrates the method in which the expressions for $\boldsymbol{p}_{i,lcl}$ (Eq. 11) were determined.

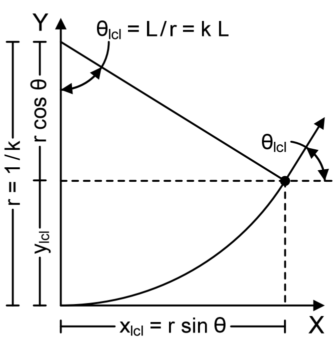


**FIGURE 2. GEOMETRIC METHOD OF DETERMINING SEGMENT DISPLACEMENT COORDINATES**

$$
\boldsymbol{p}_{i,lcl} = \begin{bmatrix} x_{i,lcl} \\ y_{i,lcl} \\ \theta_{i,lcl} \end{bmatrix} = \begin{bmatrix} \dfrac{sin(k_i L_i)}{k_i} & \dfrac{1-cos(k_i L_i)}{k_i} & k_i L_i \end{bmatrix}^T \tag{11}
$$

The coordinate transformation $\boldsymbol{T}_{i-1}$ (Eq. 12) transforms the linear coordinate to account for the total rotation of the previous disk's frame while maintaining the angular coordinate for addition to the previous angle. Though it appears similar to a rotation matrix, strictly speaking, it is not, as only two dimensions have been considered.

$$
\boldsymbol{T}_{i-1} = \begin{bmatrix} cos\,\theta_{i-1} & -sin\,\theta_{i-1} & 0 \\ sin\,\theta_{i-1} & cos\,\theta_{i-1} & 0 \\ 0 & 0 & 1 \end{bmatrix} \tag{12}
$$

Based on the definition of $\boldsymbol{p}_i$ (Eq. 10), a generalized formula for $\partial \boldsymbol{p}_i / \partial \boldsymbol{q}$ may be found using the chain rule, as shown in Eq. 13.

$$
\frac{\partial \boldsymbol{p}_i}{\partial \boldsymbol{q}} = \frac{\partial \boldsymbol{p}_{i-1}}{\partial \boldsymbol{q}} + \frac{\partial \boldsymbol{T}}{\partial \boldsymbol{q}} \boldsymbol{p}_{i,lcl} + \boldsymbol{T} \frac{\partial \boldsymbol{p}_{i,lcl}}{\partial \boldsymbol{q}} \tag{13}
$$

For $i=1$ a special case is needed, due to the recursive formulation. Equation 14 addresses this special case, in which the Jacobian mapping is simply found by taking the derivative of each row of $\boldsymbol{p}_1$ by each generalized coordinate.

$$
\frac{\partial \boldsymbol{p}_1}{\partial \boldsymbol{q}} = \begin{bmatrix} \dfrac{k_1 L_1 \, cos(k_1 L_1) - sin(k_1 L_1)}{k_1^2} & cos(k_1 L_1) & \\ \dfrac{k_1 L_1 \, sin(k_1 L_1) + cos(k_1 L_1) - 1}{k_1^2} & sin(k_1 L_1) & \boldsymbol{0}_{3\times 4} \\ L_1 & k_1 & \end{bmatrix} \tag{14}
$$

With this definition, the recursive formulation may be propagated forward for $i>2$. The second term in Eq. 13 accounts for the spatial change in the system's coordinate transformation and is calculated in Eq. 15, with the definition of $X_{k,j}$ in Eq. 16.

$$
\frac{\partial \boldsymbol{T}}{\partial \boldsymbol{q}} \boldsymbol{p}_{i,lcl} = \begin{bmatrix} X_{1,1} & X_{1,2} & X_{1,3} & X_{1,4} & X_{1,5} & X_{1,6} \\ X_{2,1} & X_{2,2} & X_{2,3} & X_{2,4} & X_{2,5} & X_{2,6} \\ 0 & 0 & 0 & 0 & 0 & 0 \end{bmatrix} \tag{15}
$$

$$
X_{k,j} = \frac{\partial T_{k,1}}{\partial q_j} x_{i,lcl} + \frac{\partial T_{k,2}}{\partial q_j} y_{i,lcl} \tag{16}
$$

The definition of coordinate transformation derivatives are found in Eq. 17. The derivatives with respect to $\theta_{i-1}$ are calculated based on the previous definition's analytical definition of $\theta_{i-1} = k_{i-1} L_{i-1}$

$$\frac{\partial T_{1,1}}{\partial q_j} = \frac{\partial T_{2,2}}{\partial q_j} = \begin{cases} -\sin\theta_{i-1}\dfrac{\partial\theta_{i-1}}{\partial q_j} & j \le 2i-2 \\ 0 & j > 2i-2 \end{cases}$$

$$\frac{\partial T_{2,1}}{\partial q_j} = -\frac{\partial T_{1,2}}{\partial q_j} = \begin{cases} \cos\theta_{i-1}\dfrac{\partial\theta_{i-1}}{\partial q_j} & j \le 2i-2 \\ 0 & j \ge 2i-2 \end{cases} \tag{17}$$

The derivatives with respect to the local position $\boldsymbol{p}_{i,lcl}$ are found in a similar manner to Eq. 14, but the location of the three-by-two submatrix varies based on the disk under consideration; Eq. 18 shows the formulation.

$$\left[\frac{\partial \boldsymbol{p}_{i,lcl}}{\partial \boldsymbol{q}}\right]_{\{:,(2i-1):(2i)\}} = \begin{bmatrix} \dfrac{k_i L_i \cos(k_i L_i) - \sin(k_i L_i)}{k_i^2} & \cos(k_i L_i) \\ \dfrac{k_i L_i \sin(k_i L_i) + \cos(k_i L_i) - 1}{k_i^2} & \sin(k_i L_i) \\ L_i & k_i \end{bmatrix} \tag{18}$$

## System Statics

Based on the kinematic analysis, three classes of static effects have been incorporated into this continuum manipulator model: gravitational, elastic and actuation.

**Gravitational Loading.** Gravity is accounted for in the model by applying a constant force in the negative global y-direction with magnitude of $mg$, as shown in Eq. 19. The planar motion simulated in this work is in the vertical plane.

$$\boldsymbol{F}_g = \begin{bmatrix} 0 & -mg \end{bmatrix}^T \tag{19}$$

**Elastic Effects.** Two types of elastic effects are considered in this model: bending and extension. Segment bending results a moment generated normal to bending. This moment is proportional to the change in segment curvature from the reference configuration $k - k_0$. The constant of proportionality is $E J_{xx}$, where $E$ is the elastic core's Young's modulus and $J_{xx}$ is the second moment of area of the elastic core's cross section.

$\boldsymbol{M}_{b,i}$ accounts for the moment loading on disk $i$ due to the segment(s) adjacent to that disk. For the first and intermediate disks on the manipulator, the loading will depend on the difference of the two segment's curvatures. For the final disk the moment is simply proportional to the opposite of the segment's bending moment, as shown in Eq. 20.

$$\boldsymbol{M}_{b,i} = \begin{cases} E J_{xx}(k_{i+1} - k_i) & i < n \\ -E J_{xx} k_n & i = n \end{cases} \tag{20}$$

The compression or extension of the continuum core results in a force generated tangent to the core's geometry at the disk(s) adjacent to the segment. This force is proportional to the change in segment length from the reference configuration $L_i - L_0$. The constant of proportionality is $EA/L_0$, where $A$ is the continuum core's cross sectional area.

$\boldsymbol{F}_{ax,i}$ accounts for the force loading on disk $i$ due to the segment(s) adjacent to that disk. As with segment bending, for the first and intermediate disks on the manipulator, the loading will depend on the difference of the two segment's lengths. For the final disk, the force is equivalent to the segment's compressive force, as shown in Eq. 21.

$$\boldsymbol{F}_{ax,i} = \begin{cases} \dfrac{EA}{L_0}(L_i - L_{i+1}) \begin{bmatrix} \cos\theta_i \\ \sin\theta_i \end{bmatrix} & i < n \\ \dfrac{EA}{L_0}(L_n - L_0) \begin{bmatrix} \cos\theta_i \\ \sin\theta_i \end{bmatrix} & i = n \end{cases} \tag{21}$$

**Actuation Loading.** In order to determine the actuation loading, the lines of action of the cable's tension along the manipulator is needed. This may be determined based on the relative positions of the cable routing holes. At the system base, the actuation cable "enters" the system at position $\boldsymbol{r}_{h,0}$ relative to the system origin. The cable routing hole positions $\boldsymbol{r}_{h,i}$ for each disk relative to that disk's center of mass (but represented in relative to the global coordinates) are found relative to the disk frame's y unit-vector ($\hat{y} = \begin{bmatrix} -\sin\theta_i & \cos\theta_i \end{bmatrix}^T$). Both are shown in Eq. 22.

$$\boldsymbol{r}_{h,0} = r_h \begin{bmatrix} 0 \\ 1 \end{bmatrix}, \quad \boldsymbol{r}_{h,i} = r_h \begin{bmatrix} -\sin\theta_i \\ \cos\theta_i \end{bmatrix} \tag{22}$$

Based on these hole positions, the position vectors from hole-to-hole ($\boldsymbol{p}_{h,i}$, Eq. 23) may be constructed. For each segment $i$, the hole-to-hole position vector may be constructed by adding the segment's local position vector $\boldsymbol{p}_i$ to the subsequent frame's hole position vector $\boldsymbol{r}_{h,i}$ and subtracting the previous frame's hole position vector $\boldsymbol{r}_{h,i-1}$. An initialization is not needed for this because of the initialization of $\boldsymbol{r}_{h,0}$.

Because only the direction of this vector is required, the unit vector $\hat{\boldsymbol{p}}_{h,i}$ is calculated.

$$\begin{aligned} \boldsymbol{p}_{h,i} &= \boldsymbol{p}_i + \boldsymbol{r}_{h,i} - \boldsymbol{r}_{h,i-1}, \\ \hat{\boldsymbol{p}}_{h,i} &= \boldsymbol{p}_{h,i} / \left\| \boldsymbol{p}_{h,i} \right\| \end{aligned} \tag{23}$$

Based on these unit vectors, the net force $\boldsymbol{F}_{act,i}$ (Eq. 24) due to the actuation on the disk may be determined by subtracting the previous segment's unit vector from the subsequent segment's for each disk, then multiplying the resultant vector by the tension $\tau$. For the final disk, the force is simply the opposite of the previous segment's unit vector

$$\boldsymbol{F}_{act,i} = \begin{cases} \tau\left(\hat{\boldsymbol{p}}_{h,i+1} - \hat{\boldsymbol{p}}_{h,i}\right) & i < n \\ -\tau\hat{\boldsymbol{p}}_{h,i} & i = n \end{cases} \tag{24}$$

Using the net force acting at the hole position on each disk, the effective force and moment acting at the disk's center of mass may be found. The equivalent force at the center of mass is equal to the original force, and the equivalent moment may be found by taking the cross product between the displacement between the two points of application ($\boldsymbol{r}_{h,i}$) and the force itself, as shown in Eq. 25.

$$\boldsymbol{M}_{act,i} = \boldsymbol{r}_{h,i} \times \boldsymbol{F}_{act,i} \tag{25}$$

Using these three classes of forces/moments, the relevant first-order mechanical effects have been incorporated into the static model of the system. An illustrative three-segment manipulator analysis will be performed to demonstrate the calculation of variables.

## IV. NUMERICAL ANALYSIS

In this section, the static analysis of Section III is numerically implemented in MATLAB, and several case studies are provided to illustrate the utility of this method.

### Numerical Implementation

MATLAB [9] was utilized to solve the set of coupled nonlinear equations presented in Eq. 5. A trust-region dogleg algorithm was chosen as a part of the 'fsolve' collection of algorithms. The solver iterated the generalized coordinates from an initial guess to minimize the magnitude of the constraint equations (Eq. 5). Due to the highly nonlinear nature of this system of equations, a set of generalized coordinate were not found to force the constraints to identically zero. However, in each case-study discussed below, the maximum error in constraint is on the order of $\sim 10^{-9}$.

The manipulator geometry and material properties utilized were inspired by a prototype used for statics validation in the literature [7], with the properties used in the following simulations defined in Table 1. In the case studies presented, a four-segment manipulator was utilized.

**TABLE 1. MANIPULATOR PROPERTIES**

| *Variable* | *Value* | *Variable* | *Value* |
|---|---|---|---|
| $n$ | 4 | $m$ | 7.782e-4 [kg] |
| $L_0$ | 0.02 [m] | $r_h$ | 0.008 [m] |
| $E$ | 2.10e11 [Pa] | $A$ | 5.027e-7 [m$^2$] |
| $I_{xx}$ | 2.029e-8 [kg-m$^2$] | $I_{zz}$ | 3.503e-8 [kg-m$^2$] |
| $J_{xx}$ | 2.011e-14 [m$^4$] | $g$ | 9.81 [m/s$^2$] |

### Numerical Results

For the initial simulation, the tension of the cable was assumed to be zero, and the static equilibrium was found in the absence of actuation and illustrated in Figure 3. As a point of comparison and in order to validate this unactuated static equilibrium, a finite element model of the manipulator using COMSOL Multiphysics [10] was generated, and the resulting disk positions have been superimposed on Figure 3.

The errors between these disk positions are presented in Table 2. The error is determined using the distances of each point from the global origin (the base of the manipulator), with the finite-element method calculation taken as the reference

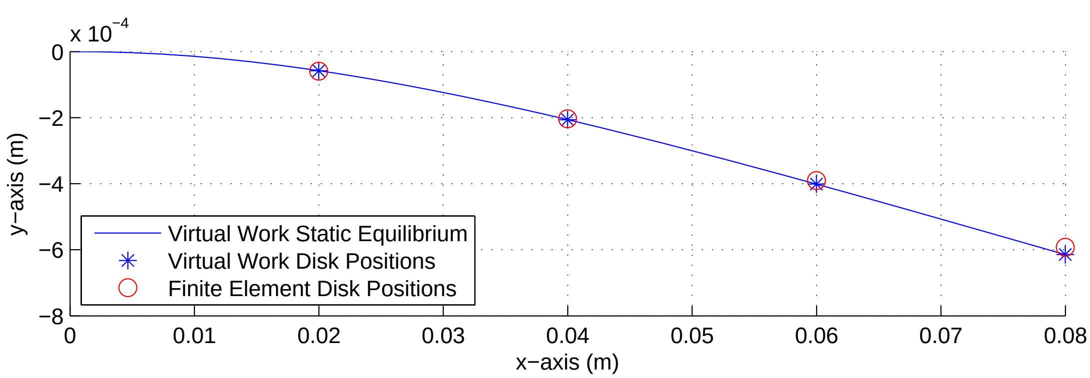


**FIGURE 3. STATIC EOUILIBRIUM WITHOUT ACTUATION**

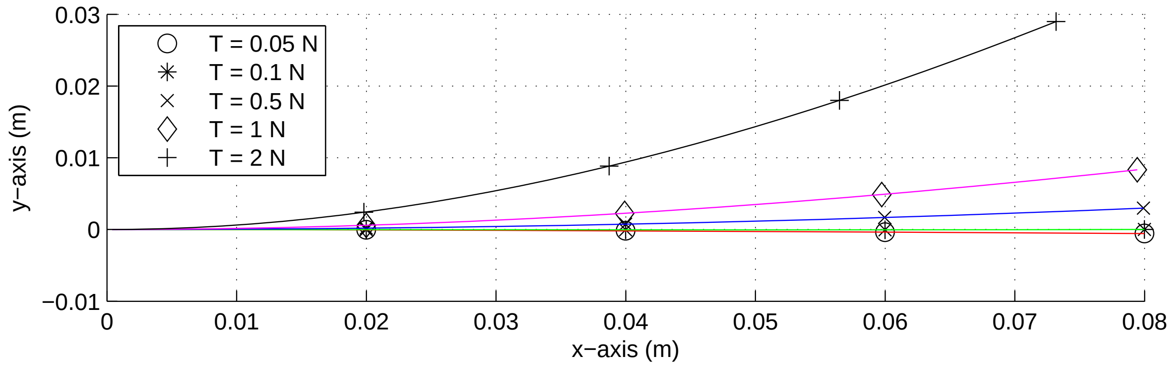


**FIGURE 4. STATIC EQUILIBRIA WITH VARIABLE CABLE TENSION**

(due to its higher fidelity). Based on these calculations, the virtual work model is a highly accurate representation of the manipulator statics, with a slight bias of the solution below the finite-element solution, with this bias increasing along the length of the manipulator. This is likely due to the method of applying the entire disk and surrounding segment mass at a single point along the manipulator in the virtual work, versus the distribution present in the finite element model.

**TABLE 2. EQUILIBRIUM DISK POSITIONS**

| *Disk* | *Virtual-Work Method (m)* | *Finite-Element Method (m)* | *Percent Error* |
|---|---|---|---|
| 1 | (1.999e-2, -5.7854e-5) | (1.9999e-2, -5.8970e-5) | 2.8268e-5 |
| 2 | (3.9999e-2, -2.0610e-4) | (3.9999e-2, -2.0347e-4) | 3.6533e-5 |
| 3 | (5.9998e-2, -4.0136e-4) | (5.9998e-2, -3.9055e-4) | 5.7060e-5 |
| 4 | (7.9997e-2, -6.1469e-4) | (7.9997e-2, -5.9276e-4) | 6.9687e-5 |

After this verification of the accuracy of the gravitational and elastic effects within the model, the effect of tensile loading was studied within the manipulator. Figure 4 shows simulations over a range of cable tensions from 0.05 N to 2 N. In the cases of 0.05 and 0.1 N, a slight sag is observed below the y = 0 axis; in these cases the cable tension is not sufficient to lift the manipulator above this horizontal datum. However, the force is observed affecting manipulator geometry with a slight upward lift of the terminal end of the manipulator at the cable attachment point. However, for tensions 0.5 N and greater, the force is sufficient to lift the manipulator above the horizontal datum, increasing curvature in all segments, with a greater increase seen in segments closest to the base.

## V. CONCLUSION

In this paper, the statics of a cable-driven continuum manipulator have been derived. Elastic, gravitational and actuation effects have been incorporated in the model, and the model has been numerically implemented and demonstrated on two numerical case studies.

Future research in this area will include three primary thrusts: (1) experimental validation of numerical results, (2) incorporation of higher-order effects in this model, and (3) development of models of continuum manipulator motion. Experimental validation will allow for the error within this model to be quantified relative to actual performance. Incorporation of higher-order effects will allow for more accurate models, and will enable modeling of manipulators with multiple actuated segments. Development of motion-based continuum manipulator models will build upon the virtual-work-based approach presented in this paper to utilize a virtual-power-based approach (Kane's method) to simulate both quasi-static and dynamic motion.

## REFERENCES

[1] Webster, III, R. J. and Jones, B. A., 2010, "Design and Kinematic Modeling of Constant Curvature Continuum Robots: A Review," International Journal of Robotics Research, **29**(13), pp. 1661-1683.

[2] Chirikjian, G. S., and Burdick, J. W., 1994, "A Modal Approach to Hyper-redundant Manipulator Kinematics," IEEE Transactions on Robotics and Automation, **10**(3), pp. 343-354.

[3] Jones, B. A., Gray, R. L., and Turlapati, K., 2009, "Three Dimensional Statics for Continuum Robotics," *IEEE/RSJ International Conference on Intelligent Robots and Systems*, St. Louis, MO, pp. 2659-2664.

[4] Rucker, D. C., Jones, B. A., and Webster, III, R. J., 2010, "A Geometrically Exact Model for Externally Loaded Concentric-Tube Robots," IEEE Transactions on Robotics, **26**(5), pp. 769-780.

[5] Xu, K., and Simaan, N., 2010, "Analytic Formulation for Kinematics, Statics and Shape Restoration of Multibackbone Continuum Robots Via Elliptic Integrals," ASME Journal of Mechanisms and Robotics, **2**, pp. 011006-1-13.

[6] Goldstein, H., Poole, C. and Safko, J., 2002, *Classical Mechanics*, Addison Wesley, San Francisco, CA, pp. 16-19, Chap. 1.

[7] Rucker, D. C., and Webster, III, R. J., 2011, "Statics and Dynamics of Continuum Robots with General Tendon Routing and External Loading," IEEE Transactions on Robotics, **27**(6), pp. 1033-1044.
[8] McMahon, W., Jones, B.A. and Walker, I.D., 2005, "Design and Implementation of a Multi-section Continuum Robot: Air-Octor," *IEEE/RSJ International Conference on Intelligent Robots and Systems*, Edmonton, Canada, pp. 2578-2585.
[9] MATLAB, Version R2009a, The MathWorks, Inc., http://www.mathworks.com/products/matlab.
[10] COMSOL Multiphysics, Version 4.2, COMSOL, Inc., http://www.comsol.com.

 